Int. J. Solids Structures Vol. 18, No. 12, pp. 1113–1128, 1982
Printed in Great Britain.

0020-7683/82/121113-16$03.00/0
Pergamon Press Ltd.

AXISYMMETRIC VISCOPLASTIC DEFORMATION BY THE BOUNDARY ELEMENT METHOD

VIJAY SARIHAN and SUBRATA MUKHERJEE
Department of Theoretical and Applied Mechanics, Thurston Hall, Cornell University, Ithaca, NY 14853, U.S.A.

(*Received* 29 *December* 1981; *in revised form* 22 *March* 1982)

Abstract—This paper presents a boundary element formulation and numerical implementation of the problem of small axisymmetric deformation of viscoplastic bodies. While the extension from planar to axisymmetric problems can be carried out fairly simply for the finite element method (FEM), this is far from true for the boundary element method (BEM). The primary reason for this fact is that the axisymmetric kernels in the integral equations of the BEM contain elliptic functions which cannot be integrated analytically even over boundary elements and internal cells of simple shape. Thus, special methods have to be developed for the efficient and accurate numerical integration of these singular and sensitive kernels over discrete elements. The accurate determination of stress rates by differentiation of the displacement rates presents another formidable challenge.

A successful numerical implementation of the boundary element method with elementwise (called the Mixed approach) or pointwise (called the pure BEM or BEM approach) determination of stress rates has been carried out. A computer program has been developed for the solution of general axisymmetric viscoplasticity problems. Comparisons of numerical results from the BEM and FEM, for several illustrative problems, are presented and discussed in the paper. It is possible to get direct solutions for the simpler class of problems for cylinders of uniform cross-section, and these solutions are also compared with the BEM and FEM results for such cases.

INTRODUCTION

The subject of this paper is the solution of boundary value problems for axisymmetric viscoplastic bodies subjected to axisymmetric mechanical loads. The boundary element method (BEM) is used to solve this class of problems.

Mukherjee and his coauthors have previously solved a number of viscoplasticity problems by the BEM. These include planar[1–4], plate bending[5], and torsion[6] problems. In most of these cases, numerical solutions to the governing integral equations have been obtained by integrating the singular kernels of the equations analytically over boundary elements and internal cells of simple shape. While the extension for planar to axisymmetric problems is carried out fairly simply in the finite element method (FEM), this is far from true for the boundary element method. The primary reason for the need of considerable effort for the BEM solution is the fact that the axisymmetric kernels contain elliptic functions which cannot be integrated analytically even over boundary elements and internal cells of simple shape. Thus, suitable methods must be developed for the efficient and accurate numerical integration of these singular and sensitive kernels over discrete elements. This aspect of the problem makes the axisymmetric case more difficult to solve than the planar problems that have been solved earlier. An important bonus of the development of accurate numerical integration techniques for singular kernels, of course, is that these ideas can then be used in other problems where analytical integration is impossible or impractical because of the need for complicated shapes of boundary elements or internal cells, or for other reasons.

The axisymmetric elasticity problem has been solved previously by the BEM and related methods by Kermanidis[7], Cruse *et al.*[8] and Shippy *et al.*[9]. A first solution for axisymmetric elastic–plastic problems has been presented by Cathie and Banerjee[10]. A BEM formulation for axisymmetric viscoplasticity problems requires, as for other viscoplasticity problems, evaluation of domain integrals. If a constitutive model for material behavior is chosen from a certain class of such models (e.g. pure creep or combined creep–plasticity constitutive equations), these integrals involve known integrands over the domain of the body and the unknowns of the body lie only on the boundary. The evaluation of these domain integrals for the displacement rate equations require special care, and the problem is more

complicated if the strain rates are evaluated by pointwise differentiation of displacement rates at a source point.

A BEM formulation and numerical implementation of the method for axisymmetric viscoplasticity problems is presented in this paper. Careful attention is paid to the accurate evaluation of integrals of singular kernels over discrete elements. The stress rates are obtained either by pointwise analytical differentiation of the displacement rates (the pure BEM method) or by elementwise numerical differentiation of these displacement rates (the Mixed method). Numerical results are obtained for several illustrative problems and the BEM, Mixed, FEM and direct solutions are compared for various cases.

GOVERNING EQUATIONS

The integral equations for the axisymmetric problem are derived from the corresponding three-dimensional equations. A few relevant three-dimensional equations are given first.

Three-dimensional equations

The starting point is the Navier equations for the displacement rates. Using decomposition of strain rates $\dot{\epsilon}_{ij}$ into elastic $\dot{\epsilon}_{ij}^{(e)}$ and nonelastic $\dot{\epsilon}_{ij}^{(n)}$ ones in the form

$$\dot{\epsilon}_{ij} = \dot{\epsilon}_{ij}^{(e)} + \dot{\epsilon}_{ij}^{(n)} \tag{1}$$

results in the equation[1] ($i, j = 1, 3$)

$$\dot{u}_{i,jj} + \frac{1}{1-2\nu}\dot{u}_{k,ki} = 2\dot{\epsilon}_{ij,j}^{(e)}. \tag{2}$$

In the above, $\dot{u}_i$ are the components of displacement rates and ν is the Poisson's ratio. Thermal strains and body forces are ignored in this paper. The boundary conditions must prescribe displacement and traction rates on the boundary of the body in the usual way.

A boundary element formulation for displacement rates can be written as ($i, j, k = 1, 3$)

$$\dot{u}_j(p) = \int_{\partial B} [U_{ij}(p, Q)\dot{\tau}_i(Q) - T_{ij}(p, Q)\dot{u}_i(Q)]\, \mathrm{d}s_Q + \int_{\partial B} 2GU_{ij}(p, Q)\dot{\epsilon}_{ik}^{(n)}(Q)n_k(Q)\, \mathrm{d}s_Q - \int_B 2GU_{ij}(p, q)\dot{\epsilon}_{ik,k}^{(n)}(q)\, \mathrm{d}v_q \tag{3}$$

in terms of the usual three-dimensional kernels U_{ij} and T_{ij}[11]. In the above, p (or P) is a source point and q (or Q) is a field point (with capital letters denoting points on the boundary ∂B and lower case letters denoting points inside the body B), G is the shear modulus, τ_i are the components of the traction vector and n_k are the components of the unit outward normal to ∂B at a point on it. Also, $\mathrm{d}s_Q$ and $\mathrm{d}v_q$ are surface volume elements, respectively.

By applying the divergence theorem, the last two terms of eqn (3) can be combined to yield the single term

$$\int_B 2GU_{ij,k}(p, q)\dot{\epsilon}_{ik}^{(n)}(q)\, \mathrm{d}v_q$$

which contains the nonelastic strain rate components rather than their derivatives. The kernel in this term, however, has a singularity of the type $1/r^2$ (in terms of the distance r between the source and field points) instead of $1/r$ in U_{ij}. Equation (3) with the last two terms replaced by the above term, is called eqn (3a).

The stress rates are obtained from the strain rates through Hooke's law and eqn (1). Several strategies can be used for the determination of strain rates from displacement rates. One is the elementwise numerical differentiation of the $\dot{u}_i$ by interpolation of the displacement rates over internal cells using suitable shape functions. Another is the pointwise analytical differentiation of displacement rates at an internal source point. Thus, eqn (3) can be differentiated at a source

point to give ($i, j, k, L = 1, 3$; L denoting differentiation with respect to an internal source point)

$$\dot{u}_{i,L}(p) = \int_{\partial B} [U_{ij,L}(p, Q)\dot{\tau}_i(Q) - T_{ij,L}(p, Q)\dot{u}_i(Q)]\, ds_Q + \int_{\partial B} 2GU_{ij,L}(p, Q)\dot{\epsilon}_{ik}^{(n)}(Q)n_k(Q)\, ds_Q - \int_B 2GU_{ij,L}(p, q)\dot{\epsilon}_{ik,k}^{(n)}(q)\, dv_q. \quad (4)$$

This method has been used to determine displacement rate gradients later in this paper. It is very important to realize that if the alternative eqn (3a) for $\dot{u}_i$ with the term involving $U_{ij,k}$ is used (as is commonly done), one must be very careful when differentiating the term $\int_B 2GU_{ij,k}\dot{\epsilon}_{ik}^{(n)}\, dv$. This is because $U_{ij,k}$ is strongly singular (singularity of $1/r^2$ in $3D$). One possibility is to evaluate the volume integral analytically for an arbitrary point p and then differentiate this integral at p. This usually requires interpolation of the nonelastic strain rates over a volume element and analytical integration of the kernal $U_{ik,k}$ over that element. This has been done successfully for planar problems [2–4]. Another alternative is to carry out convected differentiation of the integral over the region $B - B_\eta(p)$ (where $B_\eta(p)$ is a sphere or radius η centered at p) as suggested by Bui[12]. This method gives the proper residual term in the expression for the strain rate. It still leaves the problem, however, of numerically dealing with a kernel which behaves like $1/r^3$ near a source point, in case the kernel cannot be integrated analytically. Equation (4), on the other hand, has a kernel with a strongest singularity of $1/r^2$, and can be directly implemented numerically in a computer program. It does, however, have the gradient of $\dot{\epsilon}_{ij}^{(n)}$, rather than the strain rate components themselves, in the volume integral.

Axisymmetric equations

An axisymmetric body with axisymmetric loading is considered in this paper. Using polar coordinates R, θ and Z, the nonzero components of displacements, stresses and strains are u_R, u_Z, ϵ_{RR}, $\epsilon_{\theta\theta}$, ϵ_{ZZ}, ϵ_{RZ} $(= \epsilon_{ZR})$, σ_{RR}, $\sigma_{\theta\theta}$, σ_{ZZ} and σ_{RZ} $(= \sigma_{ZR})$. All dependent variables are functions of R, Z and t. Some torsion problems can be independent of θ, but these are not included in this formulation.

A boundary element formulation for displacement rates, for the axisymmetric problem, can be based on eqn (3) or on its alternate version (3a) in which the last two terms are combined together to a single volume integral. The idea is to reduce the three-dimensional equations effectively to two-dimensional ones on a generator plane of the axisymmetric body.

The coordinate system used is shown in Fig. 1. The source point is denoted by $(R, 0, Z)$ and

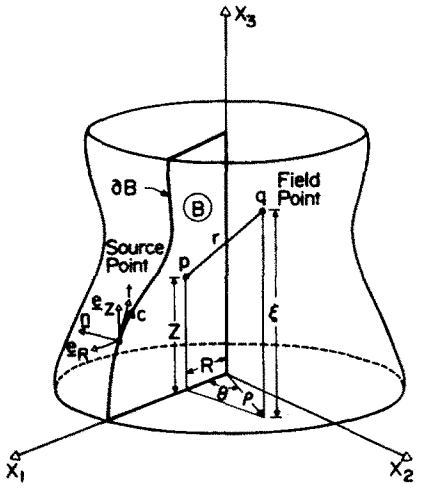

Fig. 1. Geometry of the axisymmetric problem.

the field point by (ρ, θ, ξ). Since the problem is axisymmetric, it is sufficient to choose the source point in the $x_1 - x_3$ plane. The source point coordinates are denoted here by capital letters. It can, of course, lie inside or on the surface of the body.

The BEM formulation given below is based on eqn (3a). An axisymmetric version of the three-dimensional equations can be obtained by integrating the kernels U_{ij}, T_{ij}, etc. for the field point moving around a ring with the source point fixed. This can also be done by formulating a singular body force representation of the ring loads in a direct fashion (see Cruse[8]). The first approach is used here (see Ref. [7] for related work using fictitious loads).

Integrating eqn (3a) for the field point coordinate θ between 0 and 2π results in the equation ($j = 1$ and 3, no sum over ρ or ξ):

$$\begin{aligned} u_j(p) = \int_{\partial B} & (U_{\rho j}(p, Q)\dot{\tau}_\rho(Q) + U_{\xi j}(p, Q)\dot{\tau}_\xi(Q) \\ & - T_{\rho j}(p, Q)\dot{u}_\rho(Q) - T_{\xi j}(p, Q)\dot{u}_\xi(Q))\rho_Q \, \mathrm{d}c_Q \\ & + 2G \int_B \Big(U_{\rho j,\rho}(p, q)\dot{\epsilon}^{(n)}_{\rho\rho}(q) + U_{\rho j,\xi}(p, q)\dot{\epsilon}^{(n)}_{\rho\xi}(q) \\ & + U_{\xi j,\rho}(p, q)\dot{\epsilon}^{(n)}_{\xi\rho}(q) + U_{\xi j,\xi}(p, q)\dot{\epsilon}^{(n)}_{\xi\xi}(q) \\ & + \frac{U_{\rho j}(p, q)\dot{\epsilon}^{(n)}_{\theta\theta}(q)}{\rho_q} \Big) \rho_q \, \mathrm{d}\rho_q \, \mathrm{d}\xi_q \end{aligned} \tag{5}$$

where, because of axisymmetry, $\dot{u}_R(p) = \dot{u}_1(p)$, $\dot{u}_Z(p) = \dot{u}_3(p)$, and $\mathrm{d}c = \sqrt{(\mathrm{d}\rho^2 + \mathrm{d}\xi^2)}$ is an element on the boundary of the $\rho - \xi$ plane. The boundary ∂B in this paper is that of a $R - Z$ plane and the domain B is a $R - Z$ section of the axisymmetric solid. Thus, only line integrals and area integrals must be evaluated in eqn (5). This reduces the three-dimensional problem to a two-dimensional one.

The kernels $U_{\rho 1}$, etc. are given by the equations[8]

$$\begin{aligned} U_{\rho 1}(p, q) = \frac{1}{16\pi(1-\nu)G} \frac{k}{\sqrt{(R\rho)}} \Big(& \Big(2(3-4\nu)\gamma + \frac{(Z-\xi)^2}{R\rho} \Big) K(k) \\ & - \Big(2(3-4\nu)(1+\gamma) + \Big(\frac{\gamma}{\gamma - 1} \Big) \frac{(Z-\xi)^2}{R\rho} \Big) E(k) \Big) \end{aligned} \tag{6}$$

$$U_{\xi 1}(p, q) = \frac{(\xi - Z)k}{16\pi(1-\nu)GR\rho\sqrt{(R\rho)}} \Big(RK(k) + \frac{(\rho - R\gamma)}{\gamma - 1} E(k) \Big) \tag{7}$$

$$U_{\rho 3}(p, q) = \frac{(Z-\xi)k}{16\pi G(1-\nu)R\rho\sqrt{(R\rho)}} \Big(\rho K(k) - \frac{(\rho\gamma - R)}{(\gamma - 1)} E(k) \Big) \tag{8}$$

$$U_{\xi 3}(p, q) = \frac{1}{8\pi(1-\nu)G} \frac{k}{\sqrt{(R\rho)}} \Big((3-4\nu)K(k) + \frac{(Z-\xi)^2}{2R\rho(\gamma - 1)} E(k) \Big) \tag{9}$$

where $K(k)$ and $E(k)$ are complete elliptic integrals of the first and second kind respectively and $k = \sqrt{[2/(1+\gamma)]}$. Further,

$$\gamma = 1 + \frac{((Z-\xi)^2 + (R-\rho)^2)}{2R\rho}.$$

The traction kernels are given in terms of derivatives of $U_{\rho j}$, etc. by the equations ($j = 1$ and 3)

$$\frac{1}{2G} T_{\rho j}(p, Q) = \Big(\Big(\frac{1-\nu}{1-2\nu} \Big) \frac{\partial U_{\rho j}}{\partial \rho} + \frac{\nu}{(1-2\nu)} \Big(\frac{1}{\rho} U_{\rho j} + \frac{\partial U_{\xi j}}{\partial \xi} \Big) \Big) n_\rho + \frac{1}{2} \Big(\frac{\partial U_{\rho j}}{\partial \xi} + \frac{\partial U_{\xi j}}{\partial \rho} \Big) n_\xi \tag{10}$$

$$\frac{1}{2G} T_{\xi j}(p, Q) = \Big(\Big(\frac{1-\nu}{1-2\nu} \Big) \frac{\partial U_{\xi j}}{\partial \xi} + \Big(\frac{\nu}{1-2\nu} \Big) \Big(\frac{1}{\rho} U_{\rho j} + \frac{\partial U_{\rho j}}{\partial \rho} \Big) \Big) n_\xi + \frac{1}{2} \Big(\frac{\partial U_{\rho j}}{\partial \xi} + \frac{\partial U_{\xi j}}{\partial \rho} \Big) n_\rho \tag{11}$$

where n_ρ and n_ξ are the components of the outward unit normal at the field point on the boundary in the ρ and ξ directions.

The derivatives of the displacement kernels which occur in the above equations as well as in the area integral of eqn (5) are given in Ref. [13].

The boundary integral equation when the source point p becomes a point P on the boundary ∂B of the body is ($j = 1$ and 3, no sum over ρ or ξ)

$$\begin{aligned} c_{ij}(P)\dot{u}_i(P) = \int_{\partial B} & (U_{\rho j}(P, Q)\dot{\tau}_\rho(Q) + U_{\xi j}(P, Q)\dot{\tau}_\xi(Q) \\ & - T_{\rho j}(P, Q)\dot{u}_\rho(Q) - T_{\xi j}(P, Q)\dot{u}(Q))\rho_Q \, dc_Q \\ & + 2G\int_B \Big(U_{\rho j,\rho}(P, q)\dot{\epsilon}^{(n)}_{\rho\rho}(q) + U_{\rho j,\xi}(P, q)\dot{\epsilon}^{(n)}_{\rho\xi}(q) \\ & + U_{\xi j,\rho}(P, q)\dot{\epsilon}^{(n)}_{\xi\rho}(q) + U_{\xi j,\xi}(P, q)\dot{\epsilon}^{(n)}_{\xi\xi}(q) \\ & + \frac{U_{\rho j}(P, q)\dot{\epsilon}^{(n)}_{\theta\theta}(q)}{\rho_q} \Big) \rho_q \, d\rho_q \, d\xi_q. \end{aligned} \tag{12}$$

The components of c_{ij} depend, as usual, on the geometry of the boundary at P. these components are determined indirectly and the details of this approach are discussed in a subsequent section called "Numerical Implementation".

Internal stress rates

As discussed before, the stress rates at internal points must be determined from the displacement rate gradients through Hooke's Law and eqn (1). One approach is to interpolate the displacement rates within each internal cell by suitable shape functions and then differentiate these shape functions elementwise to obtain the strain rates. This strategy, therefore, uses the boundary element method to determine displacement rates throughout the body and then a method analogous to finite elements to obtain strain rates. It will henceforth be called the mixed method. It has been used by Cathie and Banerjee [10] to solve axisymmetric plasticity problems. This method can be implemented in a simple manner but has the disadvantage of allowing discontinuities in stress rates at internal nodes and across inter-cell boundaries.

The other approach is pointwise analytical differentiation of the displacement rates at an internal source point. As mentioned before, eqn (5), which is based on eqn (3a), is not a convenient starting point for the determination of strain rates. This is because eqn (5) contains kernels like $U_{\rho j,\rho}$, which have singularities of the type $1/r$ in a two-dimensional (area) integral. It is more convenient to start, instead, from an axisymmetric version of eqn (3). This axisymmetric equation contains kernels like $U_{\rho j}$ in the area integral which have weaker logarithmic singularities. Thus, there is no problem with direct differentiation of this equation at a source point. This approach is called the "strain rate gradient method" since the area integral in this case contains gradients of nonelastic strain rates (see eqn 4). This gives the equation

$$\begin{aligned} \dot{u}_{j,L}(p) = \int_{\partial B} & (U_{\rho j,L}(p, Q)\dot{\tau}_\rho(Q) + U_{\xi j,L}(p, Q)\dot{\tau}_\xi(Q) \\ & - T_{\rho j,L}(p, Q)\dot{u}_\rho(Q) - T_{\xi j,L}(p, Q)\dot{u}_\xi(Q))\rho_Q \, dc_Q \\ & + 2G\int_{\partial B} (U_{\rho j,L}(p, Q)(\dot{\epsilon}^{(n)}_{\rho\rho}(Q)n_\rho(Q) + \dot{\epsilon}^{(n)}_{\rho\xi}(Q)n_\xi(Q)) \\ & + U_{\xi j,L}(p, Q)(\dot{\epsilon}^{(n)}_{\xi\rho}(Q)n_\rho(Q) + \dot{\epsilon}^{(n)}_{\xi\xi}(Q)n_\xi(Q)))\rho_Q \, dc_Q \\ & - 2G\int_B \Big(U_{\rho j,L}(p, q)\Big(\dot{\epsilon}^{(n)}_{\rho\rho,\rho}(q) + \frac{\dot{\epsilon}^{(n)}_{\rho\rho}(q) - \dot{\epsilon}^{(n)}_{\theta\theta}(q)}{\rho_q} + \dot{\epsilon}^{(n)}_{\rho\xi,\xi}(q) \Big) \\ & + U_{\xi j,L}(p, q)\Big(\dot{\epsilon}^{(n)}_{\xi\rho,\rho}(q) + \frac{\dot{\epsilon}^{(n)}_{\xi\rho}(q)}{\rho_q} + \dot{\epsilon}^{(n)}_{\xi\xi,\xi}(q) \Big) \Big) \rho_q \, d\rho_q \, d\xi_q \end{aligned} \tag{13}$$

where $j = 1$ and 3, $L = 1$ and 3 and there is no summation over ρ or ξ. Differentiation with respect to a capital letter denotes a source point derivative. By virtue of axisymmetry (see Fig. 1),

$$u_{R,R} = u_{1,1}, \quad u_{R,Z} = u_{1,3},$$

$$u_{Z,R} = u_{3,1}, \quad u_{Z,Z} = u_{3,3}.$$

This method requires accurate values of $\dot{\epsilon}_{ij}^{(n)}$ on the boundary ∂B, and these can be obtained from the boundary stresses. The boundary stresses can be determined accurately by using the approach discussed in the next section. Equation (13) has the drawback of requiring the divergence of the nonelastic strain rates over the domain of B. Numerical realization of these nonelastic strain rate derivatives requires piecewise interpolation of nonelastic strain rates over internal cells. This might be less accurate than direct evaluation of $\dot{\epsilon}_{ij}^{(n)}$ at internal Gauss points.

It should be noted that kernels in the boundary integrals of stress rate equations never become singular if a source point lies inside the body B.

Numerical results based on eqns (5), (12) and (13) are called BEM results later in this paper. Those based on (5), (12) and elementwise differentiation of displacement rates are referred to as being obtained from the Mixed method.

Boundary stress rates

It is very difficult to determine strain rates at a boundary point by taking the limit as $p \to P$ in eqn (13). These are best determined from a boundary algorithm which has been presented earlier for elasticity problems in cartesian coordinates by Rizzo and Shippy[14]. The method outlined below is analogous to that in Ref. [14].

The boundary integral equation is solved at a given time so that the rates of displacements and tractions are known over the entire boundary. In this discussion, piecewise straight boundary elements are considered on the boundary ∂B. The normal and tangential components of the traction rate vector are first calculated at some point P on ∂B. (P is assumed to lie at a point on ∂B where it is locally smooth.) Now

$$\dot{\sigma}_{nn} = \dot{\tau}_n, \quad \dot{\sigma}_{nc} = \dot{\tau}_c$$

where $\dot{\sigma}_{nn}$ and $\dot{\sigma}_{nc}$ are the normal and shearing components of the stress rates at P. As usual, the anticlockwise distance along the boundary element at P is denoted by c (see Fig. 1). Next, the normal and tangential components of the displacement rate vector are calculated at P and the tangential derivative of $\dot{u}_c$, $\partial \dot{u}_c / \partial c$, is obtained at P by numerical differentiation along the boundary element. The constitutive equations are written as

$$\frac{\partial \dot{u}_c}{\partial c} = \dot{\epsilon}_{cc} = \frac{1}{E}[\dot{\sigma}_{cc} - \nu(\dot{\sigma}_{nn} + \dot{\sigma}_{\theta\theta})] + \dot{\epsilon}_{cc}^{(n)} \tag{14}$$

$$\frac{\dot{u}_R}{R} = \dot{\epsilon}_{\theta\theta} = \frac{1}{E}[\dot{\sigma}_{\theta\theta} - \nu(\dot{\sigma}_{nn} + \dot{\sigma}_{cc})] + \dot{\epsilon}_{\theta\theta}^{(n)}. \tag{15}$$

The nonelastic strain rates $\dot{\epsilon}_{RR}^{(n)}$, $\dot{\epsilon}_{\theta\theta}^{(n)}$, $\dot{\epsilon}_{ZZ}^{(n)}$ and $\dot{\epsilon}_{RZ}^{(n)}$ are known at P from the stresses through an appropriate constitutive model. The strain rate $\dot{\epsilon}_{cc}^{(n)}$ is obtained from these by the usual coordinate transformation

$$\dot{\epsilon}_{cc}^{(n)} = \dot{\epsilon}_{RR}^{(n)} n_Z^2 + \dot{\epsilon}_{ZZ}^{(n)} n_R^2 - 2\dot{\epsilon}_{RZ}^{(n)} n_R n_Z \tag{16}$$

where $n_R = \mathbf{n} \cdot \mathbf{e}_R$ and $n_Z = \mathbf{n} \cdot \mathbf{e}_Z$.

The eqns (14) and (15) are linear equations which can be solved for the unknown stress rates $\dot{\sigma}_{cc}$ and $\dot{\sigma}_{\theta\theta}$. This yields the stress rates $\dot{\sigma}_{nn}$, $\dot{\sigma}_{nc}$, $\dot{\sigma}_{cc}$ and $\dot{\sigma}_{\theta\theta}$. The first three rates can be transformed back to yield the stress rates $\dot{\sigma}_{RR}$, $\dot{\sigma}_{ZZ}$ and $\dot{\sigma}_{RZ}$. Thus

$$\dot{\sigma}_{RR} = \dot{\sigma}_{nn} n_R^2 + \dot{\sigma}_{cc} n_Z^2 - 2\dot{\sigma}_{nc} n_R n_Z \tag{17}$$

$$\dot{\sigma}_{ZZ} = \dot{\sigma}_{cc} - \dot{\sigma}_{RR} \tag{18}$$

$$\dot{\sigma}_{RZ} = (\dot{\sigma}_{nn} - \dot{\sigma}_{cc}) n_R n_Z + \dot{\sigma}_{nc}(n_R^2 - n_Z^2). \tag{19}$$

FINITE ELEMENT AND DIRECT FORMULATIONS

The finite element formulation used to obtain the numerical results in this paper is that discussed in Ref. [15]. It is a standard approach based on a rate form of the principle of virtual work.

It is possible to derive a direct solution for the much simpler class of problems of cylinders of uniform circular cross-section in plane strain subjected to axisymmetric pressures. These solutions are very useful for the evaluation of the accuracy of the BEM and FEM solutions. Details of this direct method are available in many previous references (see, e.g. Refs. [16, 17]).

NUMERICAL IMPLEMENTATION OF BEM

The numerical implementation of the BEM equations and solution strategy are quite similar to those used earlier for planar problems [1–4]. An important difference between axisymmetric problems and the planar problems described in earlier references, however, is that the axisymmetric kernels can no longer be integrated analytically over boundary elements or internal cells. Thus, special methods are required for the accurate and efficient evaluation of these singular integrals. Some of these methods are discussed in this section.

The first step, as usual, is to divide the boundary ∂B of an $R-Z$ section of the cylinder into N_s boundary segments and the interior into n_i internal cells. Denoting by $\dot{u}_i(P_M)$ the components of the displacement rates at a point P which coincides with node M, a discretized version of eqn (12) can be written as (ρ, ξ not summed, $j = 1$ and 3)

$$\begin{aligned} c_{ij}(P_M)\dot{u}_i(P_M) = \sum_{N_s} \int_{\Delta c_N} & [U_{\rho j}(P_M, Q)\dot{\tau}_\rho(Q) + U_{\xi j}(P_M, Q)\dot{\tau}_\xi(Q) \\ & - T_{\rho j}(P_M, Q)\dot{u}_\rho(Q) - T_{\xi j}(P_M, Q)\dot{u}_\xi(Q)]\rho_Q \, \mathrm{d}c_Q \\ & + 2G \sum_{n_i} \int_{\Delta A_n} \Big(U_{\rho j,\rho}(P_M, q)\dot{\epsilon}^{(n)}_{\rho\rho}(q) + U_{\rho j,\xi}(P_M, q)\dot{\epsilon}^{(n)}_{\rho\xi}(q) \\ & + U_{\xi j,\rho}(P_M, q)\dot{\epsilon}^{(n)}_{\xi\rho}(q) + U_{\xi j,\xi}(P_M, q)\dot{\epsilon}^{(n)}_{\xi\xi}(q) \\ & + \frac{U_{\rho j}(P_M, q)\dot{\epsilon}^{(n)}_{\theta\theta}(q)}{\rho_q} \Big) \rho_q \, \mathrm{d}\rho_q \, \mathrm{d}\xi_q. \end{aligned} \tag{20}$$

The inclusion of $c_{ij}(P_M)$ means that boundary nodes can be placed at a corner. In the numerical implementation used here, double nodes are placed at corners to allow for jumps in tractions and normals across corners.

Suitable shape functions are now chosen for the variation of displacement and traction rates along boundary elements and for the variation of nonelastic strain rates over internal cells. This converts eqn (20) into an algebraic system of the type

$$[A]\{\dot{u}\} + [B]\{\dot{\tau}\} = \{\dot{b}\} \tag{21}$$

which, as before, must be solved for the unspecified components of the boundary rates of displacements and tractions. Next the displacement rates and finally the stress rates are obtained throughout the body and a march forward time integration scheme is used to obtain the time-histories of the displacements, stresses and strains. The special methods needed for the accurate evaluation of the various terms in eqn (20) and in eqn (13) (if it is used) are discussed next.

Evaluation of integrals of U_{ij} *over singular boundary elements*

When a source point P_M lies inside or on the edge of a boundary element Δc_N in eqn (20), this element is termed a singular element. The integrals of U_{ij} and T_{ij} over such elements require special care. The components of the kernel U_{ij} (eqns 6–9) have a singularity of the type $\ln r$ when P_M lies in Δc_N and r is the distance between P_M and Q. In such cases, it is fruitful to use the transformation $r = e^2$ which changes $\ln r \, \mathrm{d}r$ to $4e \ln e \, \mathrm{d}e$, which is regular as $e \to 0$ [18]. Regular Gaussian integration is performed after this transformation is carried out.

Evaluation of the tensor c_{ij} *and integrals of* T_{ij}

The kernel T_{ij} has a singularity of the type $1/r$ on a singular element. The singular intergals of T_{ij} and the tensor c_{ij} are best determined indirectly by the use of rigid body translation [19] and elastic inflation modes.

Rigid body translation in the Z *direction.* The elastic problem is considered here. If a rigid

body translation $u_Z = 1$ is applied to every point of the axisymmetric body, no stresses or tractions are generated in it. In this case, eqn (12) becomes ($j = 1$ and 3)

$$c_{3j}(P) = -\int_{\partial B} T_{\xi j}(P, Q)\rho_Q \, dc_Q.$$

If ∂B_c is the part of ∂B which contains P and $\partial \hat{B}$ is the rest,

$$c_{3j}(P) + \int_{\partial B_c} T_{\xi j}(P, Q)\rho_Q \, dc_Q = -\int_{\partial \hat{B}} T_{\xi j}(P, Q)\rho_Q \, dc_Q \tag{22}$$

where the l.h.s. of eqn (22) is obtained by numerical evaluation (Gaussian integration) of the nonsingular term on the right.

Inflation mode in the R *direction.* The displacement field $u_R = R$ is a possible solution of the Navier equations for the axisymmetric elasticity problem. This gives the tractions

$$\tau_R = 2(\lambda + G)n_R, \quad \tau_Z = 2\lambda n_Z$$

at a point P on the boundary ∂B. If this solution is imposed, eqn (12) becomes

$$c_{1j}(P)R_0 = \int_{\partial B} [2U_{\rho j}(P, Q)(\lambda + G)n_\rho(Q) + 2U_{\xi j}(P, Q)\lambda n_\xi(Q) - T_{\rho j}(P, Q)\rho_Q]\rho_Q \, dc_Q \tag{23}$$

which can be written as ($j = 1$ and 3, no sum on ρ or ξ)

$$\begin{aligned} c_{1j}(P)R_P + \int_{\partial B_c} T_{\rho j}(P, Q)\rho_Q^2 \, dc_Q = &\int_{\partial B} [2U_{\rho j}(P, Q)(\lambda + G)n_\rho(Q) \\ &+ 2U_{\xi j}(P, Q)\lambda n_\xi(Q)]\rho_Q \, dc_Q \\ &- \int_{\partial \hat{B}} T_{\rho j}(P, Q)\rho_Q^2 \, dc_Q. \end{aligned} \tag{24}$$

Once again, the l.h.s. of eqn (24) is obtained by numerical evaluation (Gaussian integration) of the right. The length of a boundary element on which ρ varies must be small for this method to be useful.

Evaluation of area integral

Terms like $U_{\rho j,\rho}$ in eqn (20) or (5) are singular when the source point lies inside or on an internal cell over which the integral is being evaluated. In such a situation, $U_{\rho j,\rho}$ has a $1/r_{pq}$ singularity. The following transformation is useful for the evaluation of the area integral in such cases.

Referring to Fig. 2, let $f(R, Z; \rho, \xi)$ denote a term like $U_{\rho j,\rho}\epsilon_{\rho\rho}^{(n)}$. The integral to be evaluated over a triangular internal cell is

$$I = \int_\Delta f(R, Z; \rho, \xi) \, dA = \int_\Delta f(R, Z; \rho, \xi) s \, ds \, d\psi.$$

The coordinates (ρ, ξ) of the field point q are transformed to local polar coordinates (s, ψ). If p coincides with O, f is singular with a singularity $1/s$. Otherwise, f is regular, so that $F_1 = sf$ is always regular. Writing I in terms of F_1

$$I = \int_\Delta F_1(s, \psi) \, ds \, d\psi$$

(where R, Z is suppressed since the coordinates of the source point are fixed).

First $\beta = \psi - \alpha$ is used to change the integral into

$$I = \int_{\beta_1}^{\beta_2} \int_0^{D/\cos\beta} F_2(s, \beta) \, ds \, d\beta.$$

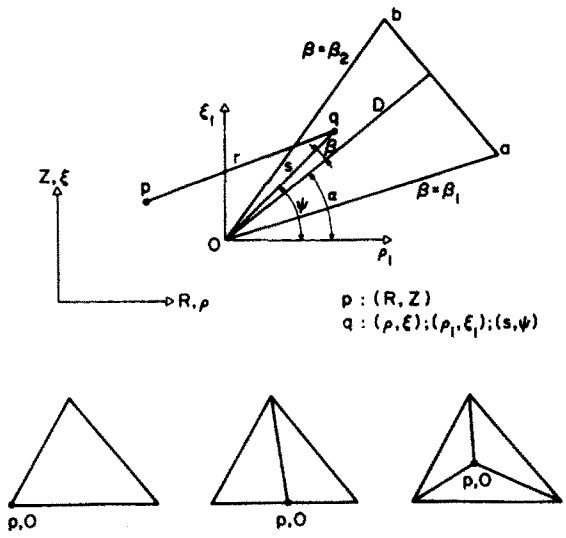

Fig. 2. Notation used for the evaluation of area integrals.

The following transformation is now used to transform the triangular cell into a unit square

$$s = \frac{\eta D}{\cos\beta}, \quad \beta = (\beta_2 - \beta_1)\phi + \beta_1.$$

Using the Jacobian of the transformation,

$$I = \int_0^1 \int_0^1 F_3(\eta, \phi) \frac{D}{\cos\beta}(\beta_2 - \beta_1)\, d\eta\, d\phi$$

$$= \int_0^1 \int_0^1 F_4(\eta, \phi)\, d\eta\, d\phi.$$

This transformed integral is evaluated by Gaussian quadrature. For the singular cases where the source points do not lie on the vertex of a triangle, the triangle can be broken up into smaller triangles as shown in Fig. 2.

The area integral in eqn (13), if it is used, can be evaluated in a similar fashion.

It is important to make sure that the integration of singular kernels over triangular internal cells is sufficiently accurate. A check which has proved useful is the numerical evaluation of both sides of the equation

$$\int_\Gamma U_{ij}\dot{\epsilon}_{ik}^{(n)} n_k\, dc = \int_A U_{ij,k}\dot{\epsilon}_{ik}^{(n)}\, dA$$

where Γ is any closed curve enclosing the area A and $\dot{\epsilon}_{ik}^{(n)}$ is divergence free. A simple choice of $\dot{\epsilon}_{ik}^{(n)}$ is $\dot{\epsilon}_{RR}^{(n)} = 1$, $\dot{\epsilon}_{\theta\theta}^{(n)} = 1$, $\dot{\epsilon}_{ZZ}^{(n)} = -2$, $\dot{\epsilon}_{RZ}^{(n)} = 0$.

NUMERICAL RESULTS—COMPARISON OF VARIOUS SOLUTIONS

Constitutive model and material parameters

A combined creep-plasticity constitutive model with state variables, that due to Hart[20], is used to describe material behavior. This model has been used many times previously by Mukherjee and his coworkers (see, e.g. Refs. [1–5, 15]. Numerical results are given in this section for 304 stainless steel at 400°C. The values of the material parameters used are the same as those given in the plate bending application[5] except that $M = 0.133 \times 10^9$ psi and $\dot{\epsilon}_0 = 3.15\ \text{sec}^{-1}$. The initial values of the state variables σ^* and $\epsilon_{ij}^{(a)}$, of the model, are taken as 17 ksi and zero, respectively.

BEM, FEM and mixed methods

The details of the various numerical methods used to get the results reported in this section are given below.

BEM (also called pure BEM). This method uses a piecewise linear description of displacements, tractions and their rates on straight boundary elements. As mentioned before, double nodes are used at corners to allow for jumps in tractions and their rates. The nonelastic strain rates are assumed to be piecewise linear on the boundary elements as well as on triangular internal cells. For the internal cells, the sampling points are placed at vertices of the triangles. The stress rates are obtained pointwise inside the body from eqn (13) and this requires the evaluation of gradients of nonelastic strain rates at points inside internal cells. Thus, some form of interpolation of these strain rates over internal cells is necessary. The boundary stress rates are obtained from the boundary stress rate algorithm described earlier.

All integrations of kernels are performed numerically. Six or twenty Gauss points are used on the boundary elements. Area integrals are evaluated by the strategy outlined in section "Evaluation of Area Integral" with a 3×3 grid Gauss points.

Mixed$_1$. In this case, the displacements and displacement rates throughout the body are obtained by the same approach as described above for the pure BEM method. The stresses and stress rates inside and on the boundary of the body, however, are obtained from a piecewise quadratic interpolation of displacements and displacement rates over triangular internal cells. The displacement rates are sampled at six points—the vertices and the mid-points of the sides of the triangular cells. There is no longer a need to interpolate nonelastic strain rates over boundary elements. Discretization of nonelastic strain rates over internal cells is carried out as for the pure BEM case. This is not strictly necessary here since nonelastic strain rate gradients need not be computed in this algorithm. However, in view of the strategy used for area integration, elimination of an interpolation scheme would require direct evaluation of nonelastic strain rates at many Gauss points for each internal cell. Thus, interpolation appears necessary as an economy measure. The boundary stress rate algorithm is not used here. Integration of kernels, required for the evaluation of displacements and their rates, are performed as in the previous case.

Mixed$_2$. This is virtually the same method as Mixed$_1$ with one important difference. Once the stress rates are obtained in B and on ∂B at a given time, the boundary stress rate algorithm is used to recalculate the stress rates at points on ∂B and these values then replace the previously calculated ones. The main idea behind Mixed$_2$ is to smooth out jumps in stresses and stress rates at the boundary nodes. This is done by central differences to obtain tangential derivatives of displacement rates.

FEM. This is the same program as discussed before [4, 15]. A piecewise quadratic interpolation of displacements and their rates are used on axisymmetric finite elements with triangular cross-sections. There is no need for shape functions for the nonelastic strain rates. Instead, these quantities are calculated directly at each time, from the constitutive model, at 7 Gauss points which lie inside a triangular element.

Elastic-solutions

Elastic solutions for the stresses in a uniform thick cylinder, in plane strain, subjected to an internal pressure of 10 ksi, have been obtained by various methods. The results, for $b/a = 1.5$ ('a' and 'b' are the inside and outside radii of the cylinder) are shown in Table 1. The FEM mesh used here is shown in Fig. 3. The dots on the same figure are the locations of the boundary nodes for the case B. Nodes = 32. The finer BEM mesh has 20 more boundary nodes

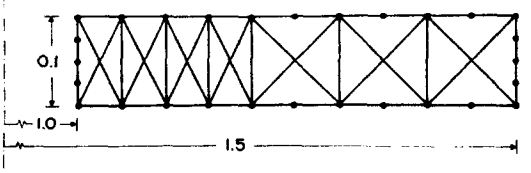

Fig. 3. BEM and FEM mesh for uniform cylinder under internal pressure. BEM: 32 boundary nodes, 28 internal cells. FEM: 73 nodes, 28 elements.

Table 1. Elastic solutions at internal points for the Lame Problem with $p_i = 10$ ksi (Stresses in psi)

R/a		Direct (Lame)	FEM (28 elements)	BEM B.Nodes = 52	BEM B.Nodes = 32
1.025	σ_{RR}	- 9133	- 9138	- 9132	- 9125
	$\sigma_{\theta\theta}$	25133	25100	25158	25232
1.075	σ_{RR}	- 7576	- 7574	- 7576	- 7576
	$\sigma_{\theta\theta}$	23576	23547	23598	23664
1.125	σ_{RR}	- 6222	- 6205	- 6224	- 6229
	$\sigma_{\theta\theta}$	22222	22202	22242	22302
1.175	σ_{RR}	- 5038	- 5007	- 5040	- 5047
	$\sigma_{\theta\theta}$	21038	21028	21056	21111
1.25	σ_{RR}	- 3520	- 3508	- 3523	- 3530
	$\sigma_{\theta\theta}$	19520	19505	19537	19586
1.35	σ_{RR}	- 1877	- 1873	- 1879	- 1886
	$\sigma_{\theta\theta}$	17877	17861	17891	17935
1.45	σ_{RR}	- 561	- 562	- 563	- 570
	$\sigma_{\theta\theta}$	16561	16546	16574	16613

placed on the faces Z = constant between the boundary nodes on Fig. 3. The BEM for this elastic problem does not require internal discretization.

All the results are seen to be very accurate (maximum deviation from the analytical solution is about 1/2%), with fine mesh BEM delivering practically the exact solution.

Initial rates for the viscoplastic problem

The viscoplastic problem requires step-wise time integration over many times steps in order to obtain the time histories of the quantities of interest. This process is expensive. Thus, it is a very good idea to compare the initial rates of displacements and stresses, as obtained from various methods, for the case of a suddenly applied load. This has been done for the uniform cylinder described above and the results are tabulated in Tables 2 and 3. The discretizations used for the FEM and BEM (with 32 boundary nodes) is shown in Fig. 3. The case of BEM with *B.* Nodes = 52 has the same distribution of internal cells.

The FEM gives the most accurate overall rates in this comparison. As expected, the finer BEM is better than the coarser one. It is felt that there are two main reasons for the difference between the BEM and FEM results. The first is that the BEM uses a piecewise linear representation of displacement rates on the boundary while the FEM has quadratic displacement rate shape functions throughout the body. The second is that the BEM has a piecewise linear representation of nonelastic strain rates over internal cells while the FEM calculates these quantities exactly at Gauss points. In fact, this alone can cause an error of as much as 7% in a nonelastic strain rate component at a point inside an internal cell. It is expected that a

Table 2. Initial radial displacement rates (in./sec) at internal points in an uniform cylinder for $p_i(0) = 10$ ksi

R/a	Direct	FEM (28 elements)	BEM (B.Nodes = 52)	BEM (B.Nodes = 32)
1.025	4469	4433	4666	4830
1.075	4078	4071	4289	4434
1.125	3883	3845	4053	4190
1.175	3725	3689	3889	4021
1.25	3556	3522	3711	3837
1.35	3395	3362	3542	3662
1.45	3273	3242	3415	3530

Table 3. Initial stress rates (psi/sec) for same case as in Table 2

R		Direct	FEM	BEM B.Nodes = 52	BEM B.Nodes = 32
1.025	$\dot{\sigma}_{RR}$	$-.8418 \times 10^{10}$	$-.1062 \times 10^{11}$	$-.9137 \times 10^{10}$	$-.9587 \times 10^{10}$
	$\dot{\sigma}_{\theta\theta}$	$-.2638 \times 10^{12}$	$-.2633 \times 10^{12}$	$-.2619 \times 10^{12}$	$-.2642 \times 10^{12}$
	$\dot{\sigma}_{ZZ}$	$-.3996 \times 10^{11}$	$-.4084 \times 10^{11}$	$-.4199 \times 10^{11}$	$-.4249 \times 10^{11}$
1.075	$\dot{\sigma}_{RR}$	$-.1551 \times 10^{11}$	$-.1639 \times 10^{11}$	$-.1745 \times 10^{11}$	$-.1890 \times 10^{11}$
	$\dot{\sigma}_{\theta\theta}$	$-.8547 \times 10^{11}$	$-.8543 \times 10^{11}$	$-.8304 \times 10^{11}$	$-.8323 \times 10^{11}$
	$\dot{\sigma}_{ZZ}$	$-.8297 \times 10^{10}$	$-.8757 \times 10^{10}$	$-.8550 \times 10^{10}$	$-.8988 \times 10^{10}$
1.125	$\dot{\sigma}_{RR}$	$-.1656 \times 10^{11}$	$-.1684 \times 10^{11}$	$-.1800 \times 10^{11}$	$-.1948 \times 10^{11}$
	$\dot{\sigma}_{\theta\theta}$	$-.4850 \times 10^{10}$	$-.4990 \times 10^{10}$	$-.1996 \times 10^{10}$	$-.1025 \times 10^{10}$
	$\dot{\sigma}_{ZZ}$	$.5543 \times 10^{10}$	$.5304 \times 10^{10}$	$.5959 \times 10^{10}$	$.5881 \times 10^{10}$
1.175	$\dot{\sigma}_{RR}$	$-.1516 \times 10^{11}$	$-.1513 \times 10^{11}$	$-.1623 \times 10^{11}$	$-.1746 \times 10^{11}$
	$\dot{\sigma}_{\theta\theta}$	$.3208 \times 10^{11}$	$.3183 \times 10^{11}$	$.3508 \times 10^{11}$	$.3558 \times 10^{11}$
	$\dot{\sigma}_{ZZ}$	$.1177 \times 10^{11}$	$.1167 \times 10^{11}$	$.1247 \times 10^{11}$	$.1267 \times 10^{11}$
1.25	$\dot{\sigma}_{RR}$	$-.1155 \times 10^{11}$	$-.1170 \times 10^{11}$	$-.1262 \times 10^{11}$	$-.1346 \times 10^{11}$
	$\dot{\sigma}_{\theta\theta}$	$.5324 \times 10^{11}$	$.5260 \times 10^{11}$	$.5597 \times 10^{11}$	$.5796 \times 10^{11}$
	$\dot{\sigma}_{ZZ}$	$.1545 \times 10^{11}$	$.1518 \times 10^{11}$	$.1593 \times 10^{11}$	$.1634 \times 10^{11}$
1.35	$\dot{\sigma}_{RR}$	$-.6458 \times 10^{11}$	$-.6469 \times 10^{10}$	$-.6910 \times 10^{10}$	$-.7387 \times 10^{10}$
	$\dot{\sigma}_{\theta\theta}$	$.5901 \times 10^{11}$	$.5840 \times 10^{11}$	$.6170 \times 10^{11}$	$.6377 \times 10^{11}$
	$\dot{\sigma}_{ZZ}$	$.1683 \times 10^{11}$	$.1664 \times 10^{11}$	$.1753 \times 10^{11}$	$.1804 \times 10^{11}$
1.45	$\dot{\sigma}_{RR}$	$-.1970 \times 10^{10}$	$-.1992 \times 10^{10}$	$-.2110 \times 10^{10}$	$-.2317 \times 10^{10}$
	$\dot{\sigma}_{\theta\theta}$	$.5776 \times 10^{11}$	$.5718 \times 10^{11}$	$.6030 \times 10^{11}$	$.6230 \times 10^{11}$
	$\dot{\sigma}_{ZZ}$	$.1716 \times 10^{11}$	$.1697 \times 10^{11}$	$.1788 \times 10^{11}$	$.1842 \times 10^{11}$

higher order interpolation of nonelastic strain rates on internal cells would give rise to a more accurate BEM solution.

Time histories of displacements and stresses for the viscoplastic problem

Time histories of displacements for various cases, obtained from different methods, are shown in Figs. 4–6 and 9. The results for axial loading of a uniform cylinder, for increasing and constant loads, respectively, are shown in Figs. 4 and 5. The results from the direct and FEM

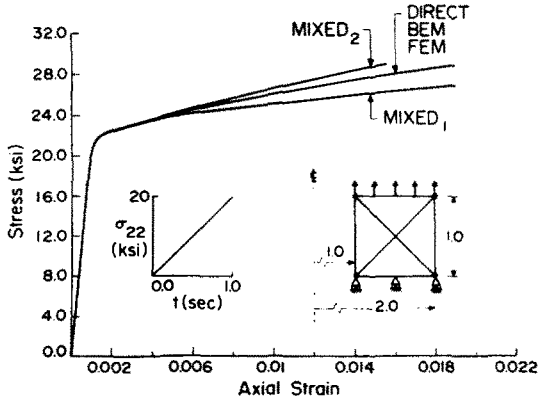

Fig. 4. Results for axial loading of a uniform circular cylinder increasing at a constant rate—comparison of various solutions. BEM: 8 boundary nodes, 4 internal cells. FEM: 12 nodes, 4 elements. $\dot{\sigma}_{22}^{\infty} = 20$ ksi/sec.

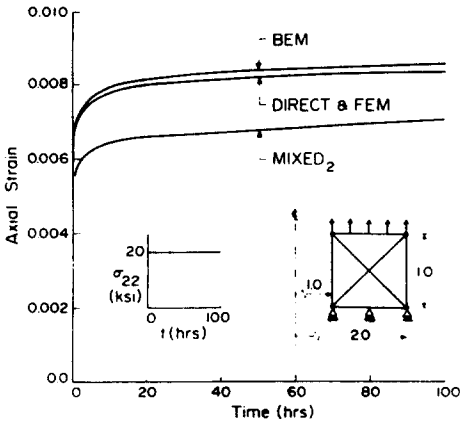

Fig. 5. Same situation as Fig. 4 but with constant remote axial load. $\dot{\sigma}_{22}^{\infty} = 20$ ksi.

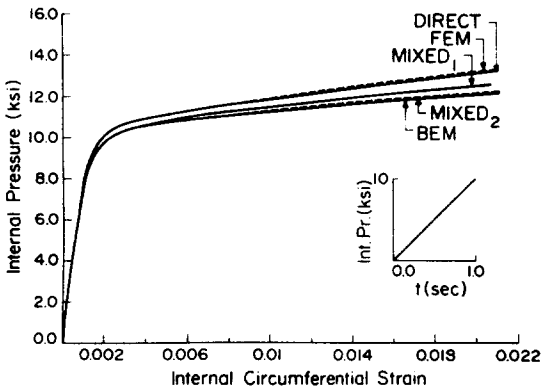

Fig. 6. Results for internal pressure on a uniform circular cylinder increasing at a constant rate—comparison of various solutions. $\dot{p} = 10$ ksi/sec. BEM and FEM mesh shown in Fig. 3.

calculations coincide in both cases for these simple problems, while the BEM results are very accurate. The Mixed$_2$ approach does relatively poorly for the creep problem in Fig. 5.

Comparisons for the case of a uniform cylinder subjected to increasing pressure (Fig. 6) are very interesting. The discretizations used for the various methods are shown in Fig. 3 with the pure BEM and mixed methods using 32 boundary nodes. Once again, the FEM comes out best. As mentioned before, the BEM errors can probably be attributed to the boundary discretization used for the displacement rates and the internal discretization for the nonelastic strain rates. Errors from the piecewise linear boundary representation of displacement rates are aggravated in the BEM and Mixed$_2$ cases which use the boundary stress algorithm, and therefore require numerical differentiation of displacement rates on the boundary ∂B. The Mixed$_1$ method, which does not use boundary stress rates, is more accurate than BEM and Mixed$_2$. In any case, the maximum BEM error is around 7% at a simulated strain in excess of 2%. This calculation requires several hundred time steps and the BEM results are considered quite satisfactory for a first attempt at this problem with very complicated kernels.

The redistribution of stresses for the same problem, obtained from the BEM algorithm, are shown in Fig. 7. The results show the expected transition from an elastic to an elastic–plastic and finally a plastic stress distribution. The crosses in this figure refer to internal points and the circles to boundary points. The boundary stresses, especially at the inner radius, become progressively less accurate with time. This is attributed to the errors from the boundary stress algorithm as mentioned above. It should be realized that errors in boundary stress rates affects boundary stresses, which, in turn, cause inaccuracies in stress rates and stresses throughout the cylinder as integration proceeds in time.

Sample results for an example of a nonuniform cylinder in plane strain are shown in Fig. 9, with the corresponding mesh shown in Fig. 8. This is representative of a portion of the core of a Gas Cooled Fast Breeder Reactor Tube (GCFR)[15]. The loading is increasing internal

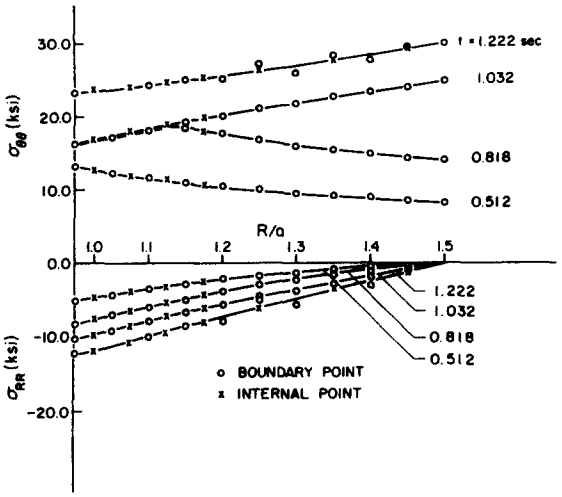

Fig. 7. Redistribution of stresses for the loading and geometry of Fig. 6. BEM solution.

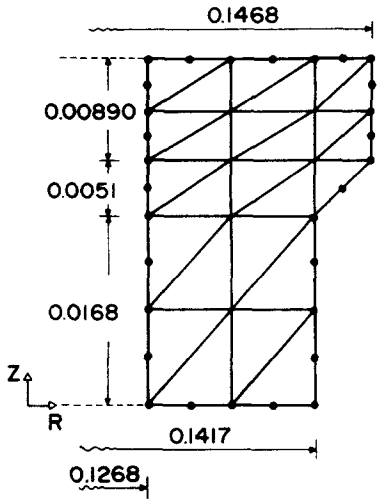

Fig. 8.

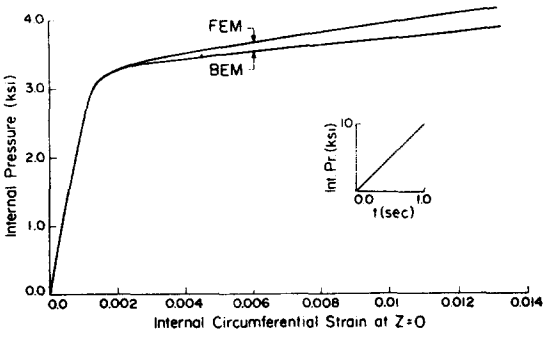

Fig. 9.

Fig. 8. BEM and FEM mesh for GCFR problem. BEM: 36 boundary nodes, 25 internal cells. FEM: 66 nodes, 25 elements.

Fig. 9. Results for GCFR tube under increasing internal pressure—comparison of BEM and FEM solutions. $\dot{p}$ = 10 ksi/sec. BEM and FEM mesh shown in Fig. 8.

pressure. The results for pressure as functions of inside circumferential strain compare well from the BEM and FEM programs. A direct solution is, of course not possible for this case.

The pure BEM has the advantage of calculating stresses and stress rates pointwise inside the body. Thus, there are no jumps in these quantities across interelement boundaries. The FEM allows such jumps across elements. The Mixed methods, as implemented here, have internal source points on the boundaries of triangular cells, in order to interpolate, rather than extrapolate, the nonelastic strain rates. This leads to large jumps in stress rates at these internal source points. These rates are directly used (without averaging) in the solution algorithm and the jumps in the rates considerably slow down the stepwise time-integration process as discussed in the next paragraph. Use of source points inside the internal cells would probably improve the performance of the Mixed$_1$ and Mixed$_2$ algorithms.

Computer times

The c.p.u. times on an IBM 370/168 computer, for the various calculations, are given in Table 4. The BEM program runs faster for all the problems. The mixed method is slow because of large jumps in stress rates at the internal nodes and due to an older inefficient algorithm for

Table 4. Computational Time Comparison. Note: E = Elastic Time, T = Total Time. *Time with NGAUSS = 10 instead of 20 for boundary integration

			BEM	MIXED$_1^*$	MIXED$_2^*$	FEM
1.	Uniaxial Tension					
	Boundary Nodes		8	8	8	
	Internal Nodes		1	5	5	13
	Elements		4	4	4	4
	a) Extension					
	C.P.U. time (secs)	E	0.727**	0.855	0.857	0.112
		T	4.783	23.602	12.536	7.718
	b) Creep					
	C.P.U. time (secs)	E	0.728**	0.88	0.867	0.121
		T	11.654	61.807	36.876	29.172
2.	Internal Pressure					
	Boundary Nodes		32	28	28	
	Internal Nodes		7	41	41	73
	Elements		28	28	28	28
	C.P.U. time (secs)	E	7.709***	22.972	23.070	0.83
		T	42.495	674.457	614.181	75.046
3.	GCFR tube					
	Boundary Nodes		36			66
	Internal Nodes		6			66
	Elements		25			25
	C.P.U. time (secs)	E	8.675***			0.468
		T	38.660			44.288

*Times are with 20 Gauss points for the elastic solution and an older inefficient algorithm for the domain integral

**Elastic Time with 20 Gauss points.

***Elastic Time with 6 Gauss points.

The mixed times have not been modified because they were considerably larger than for the pure BEM even for the same numbes of Gauss points and similar volume integral algorithm.

evaluating the domain integral. However the Mixed method was considerably slower than the pure BEM even under similar conditions.

Summary and conclusions

The primary conclusions that are derived from this research are as follows:

(a) The boundary element method has been used to obtain solutions to this difficult class of nonlinear problems. The numerical implementation of the method needs special care for the evaluation of singular integrals and for the accurate determination of stresses and stress rates.

(b) The FEM, BEM and Mixed methods have been compared with a direct solution for a set of problems for uniform cylinders. For the same mesh, the BEM, with piecewise linear shape functions on the boundary, is somewhat less accurate than the FEM which uses piecewise quadratic shape functions. The present BEM program runs faster than the FEM. It is expected that the Mixed times per time-step can be greatly improved by using the more efficient computational strategy used in pure BEM.

(c) This experience in the accurate numerical evaluation of singular integrals and stresses should prove to be very valuable in further applications of the BEM to problems where analytical integration of kernels is impossible or impractical.

Future directions

It should be emphasized that this is a first BEM attempt at solving this complicated class of problems and the implementation of the BEM can, no doubt, be greatly improved. Possible directions that can be followed are given below.

For the pure BEM:

(a) Use of higher order shape functions for the boundary displacement rates. A related idea is to retain, say, a piecewise linear boundary representation of displacement rates but to use a higher order boundary interpolation function after the displacement rates have been obtained at the boundary collocation points. This approach does not require too much additional effort but should improve the numerically calculated values of tangential derivatives of displacement rates considerably.

(b) Use of higher order interpolation functions for nonelastic strain rates over internal cells. This appears essential if the BEM accuracy is to be made comparable to FEM calculations.

For the Mixed methods:

The best, but possibly expensive, suggestion here is to drop the piecewise description on nonelastic strain rates over internal cells completely. Instead, the nonelastic strain rates should be evaluated at internal Gauss points directly from the constitutive model, as is done in the FEM program.

Acknowledgements—This research was supported by grant no. CME-7918658 of the National Science Foundation with Cornell University. Sincere thanks are expressed to Dr. M. Morjaria for many valuable discussions.

REFERENCES

1. V. Kumar and S. Mukherjee, A boundary-integral equation formulation for time-dependent inelastic deformation in metals. *Int. J Mech. Sci.* **19**, 713 (1977).
2. S. Mukherjee and V. Kumar, Numerical analysis of time-dependent inelastic deformation in metallic media using the boundary-integral equation method. *ASME J. Appl. Mech.* **45**, 785 (1978).
3. M. Morjaria and S. Mukherjee, Improved boundary-integral equation method for time-dependent inelastic deformation in metals. *Int. J. Numerical Meth. Engng* **15**, 97 (1980).
4. M. Morjaria, V. Sarihan and S. Mukherjee, Comparison of boundary element and finite element methods in two-dimensional inelastic analysis. *Res. Mechanica* 1, 3–20 (1980).
5. M. Morjaria and S. Mukherjee, Inelastic analysis of transverse deflection of plates by the boundary element method. *ASME J. Appl. Mech.* **47**, 291 (1980).
6. S. Mukherjee and M. Morjaria, Comparison of boundary element and finite element methods in the inelastic torsion of prismatic shafts. *Int. J. Numerical Meth. Engng* **17**, 1576 (1981).
7. T. Kermanidis, A numerical solution for axially symmetrical elasticity problems. *Int. J. Solids Structures* **11**, 493 (1975).
8. T. A. Cruse, D. W. Snow and R. B. Wilson, Numerical solutions in axisymmetric elasticity. *Comput. Structures* **7**, 445 (1977).
9. D. J. Shippy, F. J. Rizzo and R. K. Nigam, A boundary integral equation method for axisymmetric elastostatic bodies under arbitrary surface loads. *Innovative Numerical Analysis for the Engineering Sciences* (Edited by R. Shaw *et al.*), p. 423. University of Virginia Press, Charlottesville, Virginia (1980).
10. D. N. Cathie and P. K. Banerjee, Numerical solutions in axisymmetric elastoplasticity. *Innovative Numerical Analysis for the Applied Engineering Sciences* (Edited by R. Shaw *et al.*), p. 331. University of Virginia Press, Charlottesville, VA (1980).
11. T. A. Cruse, Numerical solution in three-dimensional elastostatics. *Int. J. Solids Structures* **5**, 1259 (1969).
12. H. D. Bui, Some remarks about the formulation of three-dimensional thermoelastoplastic problems by integral equations. *Int. J. Solids Structures* **14**, 935 (1978).
13. V. Sarihan, Ph.D. Thesis. Department of Theoretical and Applied Mechanics, Cornell University. (Expected 1982).
14. F. J. Rizzo and D. J. Shippy, A formulation and solution procedure for the general nonhomogeneous elastic inclusion problem. *Int. J. Solids Structures* **4**, 1161 (1968).
15. M. Morjarja and S. Mukherjee, Finite element analysis of time-dependent inelastic deformation in the presence transient thermal stresses. *Int. J. Numerical Meth. Engng* **17**, 909 (1981).
16. S. Mukherjee, Thermoviscoplastic response of cylindrical structures using a state variable theory. *Mechanical Behavior of Materials—Proc. ICM* 3. Cambridge, England (Edited by K. J. Miller and R. F. Smith), Vol. 2, p. 233. Pergamon Press, Oxford (1979).
17. G. W. Wire, D. R. Duncan, N. S. Cannon, G. D. Johnson, P. S. Alexopoulos, S. Mukherjee and C.-Y. Li, A state variable analysis of inelastic deformation of thin-walled tubes. *ASME J. Engng Materials Technology* **103**, 305 (1981).
18. D. J. Shippy. Private communication.
19. R. J. Rizzo and D. J. Shippy, An advanced boundary integral equation method for three-dimensional thermoelasticity. *Int. J. Numerical Meth. Engng* **11**, 1753 (1977).
20. E. W. Hart, Constitutive relations for the nonelastic deformation of metals. *ASME J. Engng Materials Technology* **98**, 193 (1976).